



A Nanocrystalline NiO Thin-Film Electrode Prepared by Pulsed Laser Ablation for Li-Ion Batteries

Ying Wang and Qi-Zong Qin^{*,*}

Department of Chemistry, Laser Chemistry Institute, Fudan University, Shanghai 200433, China

Nanocrystalline NiO thin-film electrodes were prepared by reactive pulsed laser ablation of a metallic Ni target in an oxygen ambient. X-ray diffraction (XRD) and scanning electron microscopy measurements demonstrated that the films deposited on stainless steel substrate exhibited nanocrystalline structure with average particle size of ~30 nm. Electrochemical properties of NiO films were examined by cyclic voltammetry and charge-discharge measurements. Excellent electrochemical performance, a reversible capacity as high as 700 mAh/g in the range of 0.01-3.0 V at high current density (80 $\mu\text{A}/\text{cm}^2$) with a high capacity retention up to 100 cycles, could be achieved with optimized NiO films. The improved specific capacity, discharge rate, and cycling performance might be related to the nanosized character of the thin-film electrode of NiO. Combining the XRD and X-ray photoelectron spectroscopy results, we proposed an electrochemical replacement reaction mechanism for the nanocrystalline NiO film with lithium during the discharge/charge processes. This NiO thin film could be used as a promising anode material for all-solid-state thin film rechargeable Li-ion batteries.

© 2002 The Electrochemical Society. [DOI: 10.1149/1.1481715] All rights reserved.

Manuscript submitted September 26, 2001; revised manuscript received January 16, 2002. Available electronically May 16, 2002.

Nanostructured materials often exhibit properties that are drastically different from those of conventional materials. In search of novel electrode materials for Li-ion batteries, nanostructured anode and cathode materials have been widely studied in recent years. It has been demonstrated that the charge/discharge rate, specific capacity, and cycling performance of nanostructured electrodes can be obviously improved compared with conventional electrodes made of the same materials.^{1,2} For example, the nanosized silicon composite anode materials fabricated by high-energy mechanical milling exhibited high electrochemical capacity and good lithium-ion transport dynamics.^{3,4} In addition, nanostructured anode and cathode materials were successfully fabricated using the template-synthesized method, and they also exhibited good electrochemical performance.⁵⁻⁷ These dramatically improved effects of nanostructured electrodes could be attributed to the high specific surface area and the short diffusion distance for Li-ion transport in the solid state.

Recently, Tarascon's group reported that nanosized transition metal oxides (MO, where M is Co, Ni, Fe, and Cu) were found to be promising anode materials with excellent electrochemical performance for lithium ion batteries.⁸⁻¹⁰ Since the rock-salt structured crystal of 3d transition metal oxides have no empty site for lithium ions to intercalate into, nor can it form alloy with lithium, they proposed a completely new mechanism different from the classical ones. This mechanism involves the reversible formation and decomposition of Li_2O , accompanying the reduction and oxidation of metal nanoparticles in the range 1-5 nm. Meanwhile Dahn's group¹¹ investigated the electrochemical displacement reaction of metal oxides, including $\alpha\text{-LiFeO}_2$, $\beta\text{-Li}_3\text{FeO}_4$, and CoO with lithium using *in situ* X-ray diffraction (XRD) and *in situ* Mössbauer measurements. From the data of *in situ* XRD measurements, they proposed an attractive mechanism for the reaction between lithium and CoO, in which cobalt oxide is immediately decomposed to form lithia and the reduced Co metal during discharge, and cobalt metal displaces lithium in lithium oxide to form CoO and metallic lithium during charge. This process resembles an ion-exchange process, where the Co^{2+} ions formed by the oxidation of the cobalt metal replace the lithium ions in the Li_2O lattice during cell charging.

Nickel oxide (NiO) with rock salt structure is an attractive material for antiferromagnetic devices, electrochromic electrodes, p-type transparent conducting films, chemical sensors, and active electrode material of nickel battery systems.¹²⁻¹⁶ NiO thin films have been prepared by many techniques, such as radio frequency (rf) sputtering with a nickel or nickel oxide target, pulsed laser ablation

(PLA) with a nickel oxide target, thermal evaporation, metallorganic chemical vapor deposition (MOCVD), and electrochemical deposition.¹⁷⁻²¹ Of these, PLA has proven a powerful method to prepare the thin films of pure and composite metal oxides. This method has been successfully used for preparing thin-film electrodes of LiCoO_2 , LiMn_2O_4 , and V_2O_5 .²²⁻²⁴ We have also demonstrated that the nanosized transition metal oxides such as Ta_2O_5 , Nb_2O_5 , TiO_2 , and tin composite oxide (TCO) with good electrochemical and electrochromic properties can be prepared by the PLA method.²⁵⁻²⁸ Recent laser ablation experiments have shown that the laser wavelength, intensity, ambient gas pressure, and target-substrate distance are important experimental conditions required to control the particle size distributions of the nanocrystalline semiconductor films.^{29,30} Here we employed the reactive PLA method to fabricate nanocrystalline NiO thin films with an average particle size of about 30 nm. As we know, most previous works dealing with nanosized electrode materials were investigated with nanosized metal oxides of a few hundred nanometers, and only relatively few studies focused on the novel electrochemical behavior of real nanostructured oxides (<100 nm). The motivation of this paper is to verify the excellent electrochemical performance of the thin-film electrode of nanosized transition-metal oxides by examining the nickel oxide (NiO) thin film composed of 30 nm nanoparticles. To our knowledge, this is the first report using the PLA method to prepare nanocrystalline NiO films, which can deliver a high specific capacity of ~700 mAh/g with good capacity retention. A new electrochemical mechanism, involving the electrochemical displacement reaction of lithium with NiO and the reduction/oxidation of nickel metal, is proposed to explain the electrochemical behavior of NiO film electrode. Our results may be helpful to develop new electrode materials for all-solid-state thin-film rechargeable Li-ion batteries.

Experimental

Nanocrystalline NiO films were prepared by reactive PLA in an oxygen ambient using a pure nickel target. A detailed description of PLA apparatus has been reported elsewhere.²⁷ In our experiments, a 355 nm pulsed laser beam was provided by the third harmonic frequency of a Q-switched Nd:YAG laser (yttrium aluminum garnet, Spectra Physics GCR-150) with a laser fluence of ~2 J/cm^2 and a repetition rate of 10 Hz. The incident angle between the laser beam and the target surface normal was 45°. The typical ambient O_2 gas pressure was controlled at 40 Pa by a needle valve. During deposition, the target was rotated and the substrate was mounted on a holder. The distance between pure metallic nickel target and substrate was 30 mm. The NiO film was deposited on a stainless steel substrate heated to 600°C. After deposition NiO film was annealed

* Electrochemical Society Active Member.

† E-mail: qzqin@fudan.ac.cn

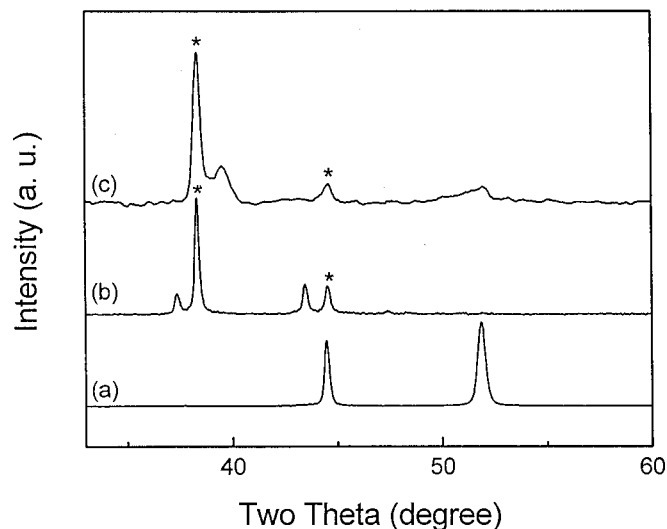


Figure 1. XRD patterns: (a) metallic Ni target, (b) NiO thin-film deposited on a stainless steel substrate, and (c) NiO thin film used as an electrode in the NiO film/Li cell discharged to 0.01 V. (*) Au-coated Si(100) substrate.

in an O_2 ambient at 300°C for 2 h. In some cases, the film was deposited on Si(100) or Au-coated Si(100) substrate for scanning electron microscopy (SEM) and XRD measurements. The film deposition rate estimated by the thickness of as-deposited film and ablation duration was found to be about 2 nm/min.

XRD patterns of the NiO thin films were determined by using a Rigata/max-C diffractometer with $\text{Cu K}\alpha$ radiation. The film morphology was characterized by a Cambridge S-360 SEM. X-ray photoelectron spectra (XPS) were obtained on a Perkin Elmer PHI 5000C ESCA system with monochromatic $\text{Al K}\alpha$ (1486.6 eV) irradiation. The XRD and XPS samples of the lithiated NiO film were prepared by disassembling the cell, rinsing the film electrode with dimethyl carbonate (DMC) to remove electrolyte, and drying the film at room temperature in an Ar-filled glove box. Then the film electrode was put in an argon-filled bag and opened right before XRD and other measurements. The film thickness was measured by a profilometer (Tencor Alpha-Step 200).

For the electrochemical measurements, two-electrode and three-electrode cells were employed with the deposited NiO thin film as working electrode, and two lithium sheets as both counter and reference electrodes. The electrolyte consisted of 1 M LiPF_6 in a non-aqueous solution of ethylene carbonate (EC) and DMC with a volume ratio of 1:1 (Merck). The cells were assembled in an Ar-filled glove box. Charge-discharge measurements were performed at room temperature with a Land BT 1-40 battery test system. The cells were cycled between 0.01 and 3.0 V vs. Li/Li^+ at different current densities from 10 to $100 \mu\text{A}/\text{cm}^2$. Cyclic voltammetric measurements were carried out with a CHI660a electrochemical work station (CHI Instruments). The measurements were performed by a computer-controlled potentiostat and galvanostat at room temperature.

Results

In order to examine the crystallinity of the NiO film prepared by PLA before and after the first discharge, XRD measurements of the metallic Ni target and NiO film were performed under different experimental conditions. As shown in Fig. 1a, the diffraction peaks of Ni target appear at 2θ of 44.48° and 51.87° , which are attributed to (111) and (200) reflections of metallic Ni, respectively. The diffraction pattern of NiO film deposited on the stainless steel substrate shown in Fig. 1b can be characterized by a cubic structure of NiO with two peaks at 37.41° and 43.47° , which corresponds to (111) and (200) reflections, respectively.^{17,31} Since the background peaks from the stainless steel substrate were removed, there was no other dif-

fraction peaks corresponding to pure Ni and other Ni-containing compounds. The average crystalline size of NiO particles on the film surface was estimated by measuring the width of the XRD peaks, which was used in the Scherrer equation. The average size of NiO particles was found to be approximately 30 nm. To examine changes of the nanocrystalline NiO during the electrochemical process, the NiO film deposited on Au-coated Si(100) substrate was discharged in a NiO film/Li cell. Figure 1c presents a significant change in the observed XRD pattern of the deposited NiO film after being discharged to 0.01 V. It can be seen that characteristic diffraction peaks of the NiO film vanished, only one peak appeared at about 52° which can be assigned to (200) reflections of metallic Ni, and another peak at 44.5° for Ni is overlapped with the broad diffraction peak from the Au-coated Si(100) substrate. The size of Ni particles was found to be about 8-10 nm. This result implies that the nanocrystalline NiO reacted with Li, leading to the formation of metallic Ni after the first discharge.

The morphologies of the NiO films deposited on the Si(100) and stainless steel substrates as well as the film electrode after electrochemical cycling were examined by SEM. As shown in Fig. 2A, the nanocrystalline NiO particles deposited on a Si(100) substrate appear to be dense, fairly round, and uniformly distributed on the surface. Their average size is found to be approximately 30 nm, which is consistent with that estimated from the XRD data. A similar result is shown in Fig. 2B, in which the NiO was deposited on a stainless steel substrate. It implies that the NiO film with uniformly distributed nanosized particles prepared by the PLA method is irrelevant to the substrate we used. In order to examine any changes in the nanocrystalline NiO particles during electrochemical cycling, the morphology of the film was also examined after cycling. As shown in Fig. 2C, when the NiO film electrode was discharged/charged at $80 \mu\text{A}/\text{cm}^2$ after 60 cycles, an obvious agglomeration took place. Compared to Fig. 2B, it is obvious that not only the larger-sized particles appear to be in the range of 150-200 nm, but also the shape of these particles changes obviously from round to needle-like shape. It has been found that the agglomeration of the nanosized particles caused by the electrochemical reactions with lithium is a common phenomenon, but the nature of this process is unclear, and we discuss it in the next section. The SEM image in Fig. 2D shows a cross-sectional view of the NiO film deposited on a Si(100) substrate for 2 h. The thickness of the dense nanocrystalline NiO film was found to be approximately 250 nm, which is close to the film thickness measured by the profilometric method.

The voltage-specific capacity profiles of the NiO film/Li cells were performed by constant current charge/discharge measurements. Figure 3 shows the first three cycling curves of NiO film/Li cell measured between 0.01 and 3.0 V vs. Li/Li^+ at $10 \mu\text{A}/\text{cm}^2$. In the initial discharge, the potential drops rapidly to reach a well-pronounced plateau at about 0.4 V, followed by a gradual decrease to 0.01 V. The irreversible discharge capacity can be delivered to be 1800 mAh/g, which correspond to about 5 Li ions reacted with the NiO film electrode. The first charge proceeds with a higher voltage and less capacity. In the second discharge, the plateau appears at about 0.9 V, and then the amplitude of the plateau reduces not obviously in the subsequent discharge curves. The subsequent charged plateau presents at about 2.0 V, which exhibits considerable polarization compared to the discharge process. Our result revealed that there was little change in the voltage-capacity profiles for the subsequent cycles, and a high reversible capacity of 700 mAh/g was achieved at a current density of $80 \mu\text{A}/\text{cm}^2$. These discharge and charge curves for the NiO film/Li cell are similar to those for the 3d transition oxides MO powder/Li cells reported previously.⁸⁻¹¹ Nevertheless, compared with other anode materials the voltage ranges of the discharge and charge curves are wider for these metal oxide electrodes. In addition, the irreversible capacity for the NiO film-based lithium cell is much higher than that for the NiO powder lithium cell upon the first discharge.

To further study the electrochemical properties of the NiO film, the film electrodes were discharged and charged at different current

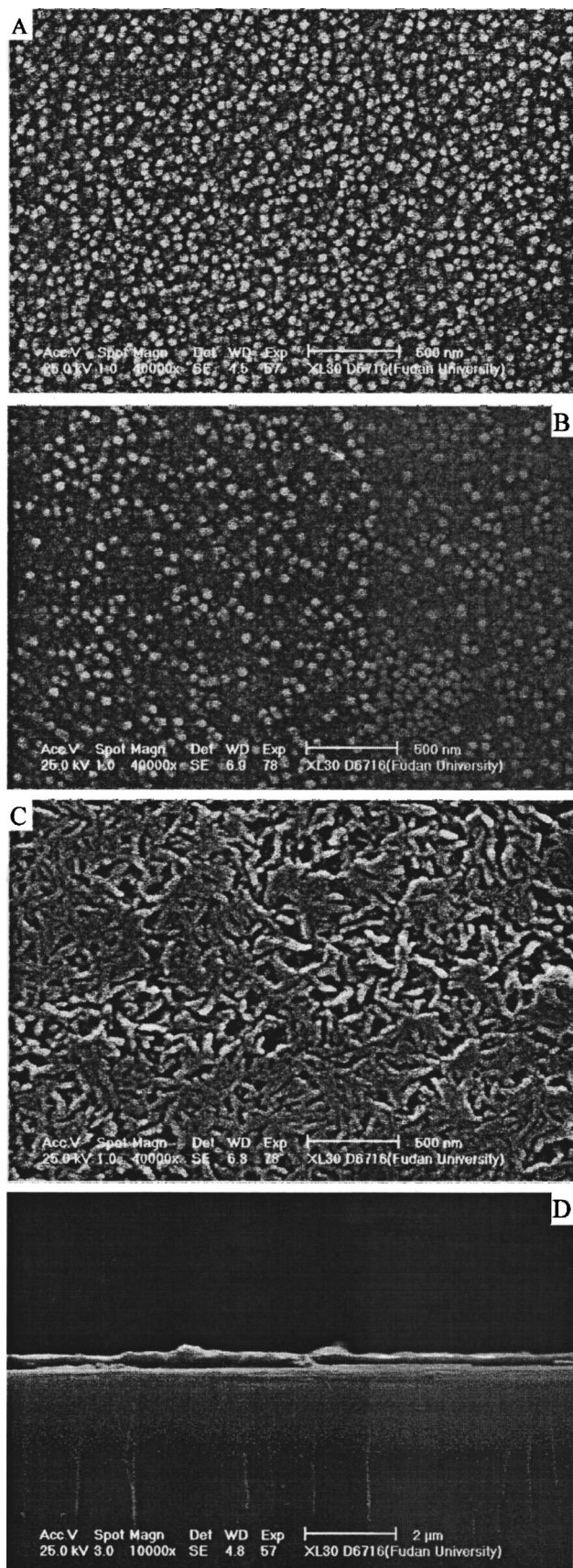


Figure 2. SEM images for as-deposited NiO thin films: (A) deposited on a Si(100) substrate, (B) deposited on a stainless steel substrate, (C) NiO film used as an electrode after 60 cycles at $80 \mu\text{A}/\text{cm}^2$, and (D) a cross-sectional view of a NiO film deposited on a Si(100) substrate for 2 h.

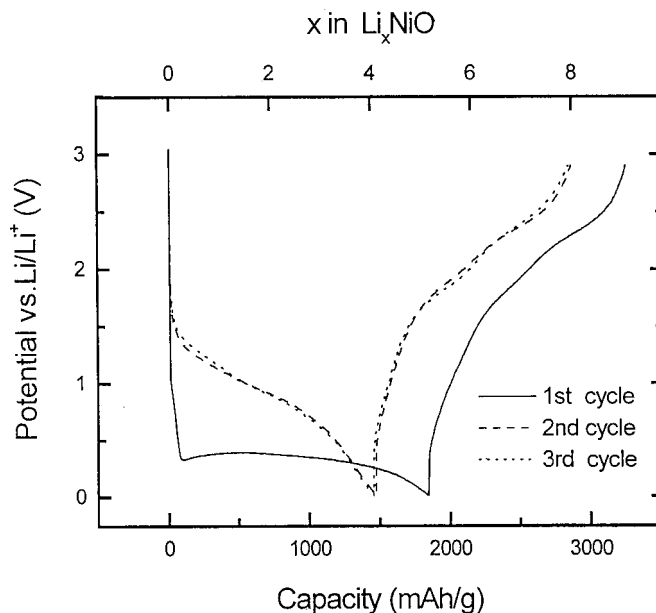


Figure 3. Voltage-capacity profiles for the NiO film/Li cell cycled between 0.01 and 3.0 V at a current density of $10 \mu\text{A}/\text{cm}^2$.

densities in the range $10\text{--}100 \mu\text{A}/\text{cm}^2$. The dependence of reversible capacity on the cycle number and the current density is presented in Fig. 4. It can be seen that the specific capacity decreases rapidly in the first 20 cycles, then slowly decays, and finally remains nearly a constant capacity after 100 cycles. At a current density of $20 \mu\text{A}/\text{cm}^2$, the NiO film electrode exhibits a large reversible capacity of 720 mAh/g , which corresponds to about 2 equiv mol of Li ion per unit mole of NiO.

From the data in Fig. 4 the specific capacity of the NiO film electrode as a function density after 100 cycles for NiO film/Li cell is shown in Fig. 5. It can be seen that the reversible capacity decreases with increasing the current density. However, this film electrode exhibits a capacity as high as about 600 mAh/g , even when cycling at $100 \mu\text{A}/\text{cm}^2$. Apparently, the reversible capacity of the NiO film electrode is quite high compared with the theoretical capacity of graphite (372 mAh/g).³² Because the density of nickel oxide ($6.67 \text{ g}/\text{cm}^3$) is larger than that of graphite ($2.26 \text{ g}/\text{cm}^3$), the

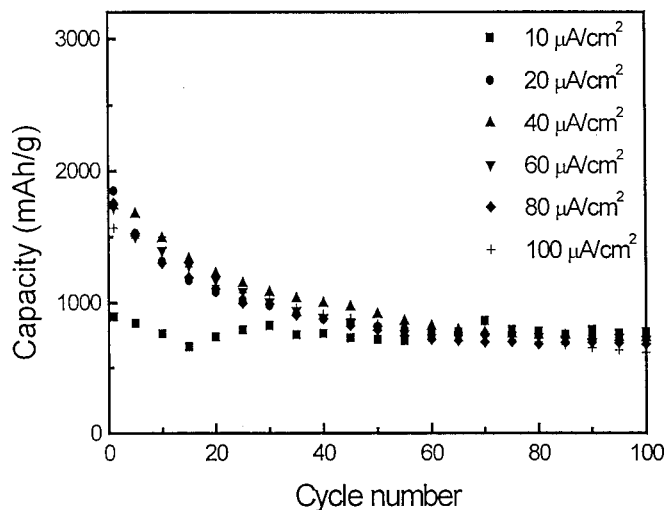


Figure 4. Discharge capacity of the NiO thin-film electrode as a function of the cycle number and current density cycled between 0.01 and 3.0 V.

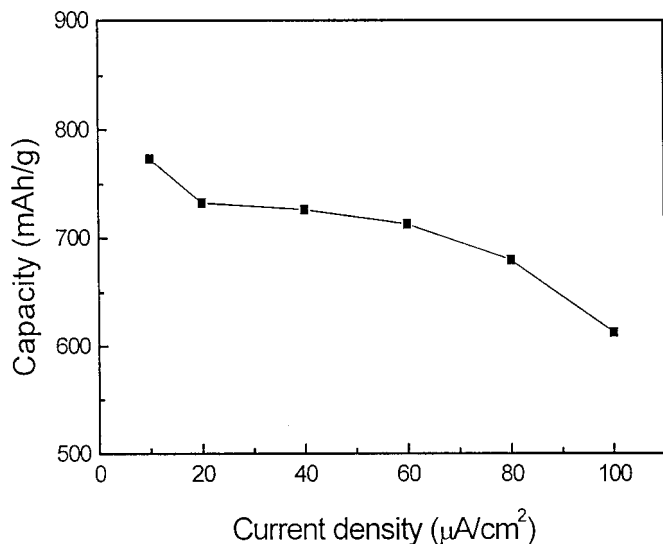


Figure 5. Specific capacity of the NiO film electrode as a function of current density after 100 cycles for NiO film/Li cell.

volumetric capacity of NiO is about six times that of graphite. The improved electrochemical performance of the nanocrystalline NiO film electrode could be attributed to the film consisting of particles having sizes ranging about 30 nm and the highly ordered structure of NiO in the film electrode.

Cyclic voltammetric (CV) measurements were performed at a sweep rate of 5 mV/s to examine the electrochemical properties of the NiO film electrode. Figure 6 presents the CV curves cycled between 0 and 3.5 V for the film electrode after different cycles. It can be seen that in the second cycle a broad anodic peak is observed at about 2.3 V on charge, and a fairly sharp cathodic peak is located at 0.9 V vs. Li/Li⁺ on discharge. These two peaks could be attributed to the one-step reversible electrochemical oxidation and reduction of NiO with lithium in the film electrode. Furthermore, some modifications of the CVs appear in the cathodic peak upon the 5th and 10th cycles, and the peak potential slightly decreases to 0.7 and 0.6 V, respectively. However, the NiO film electrode showed good reversibility and repeatability after 20 cycles. The effect of the scan rates on the CV profile is complicated and an investigation is in progress.

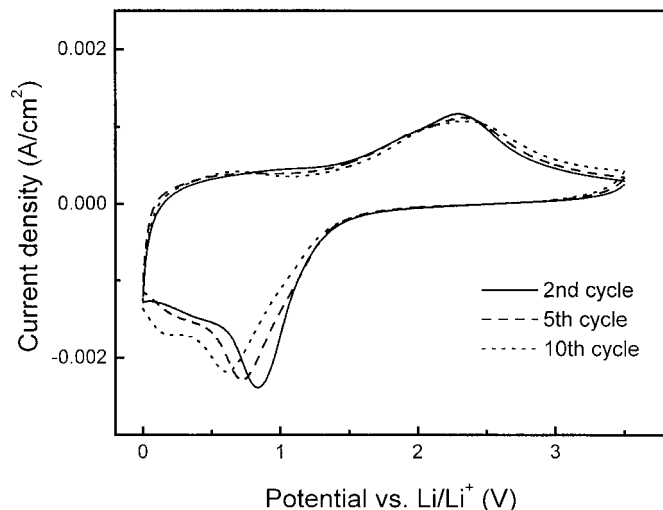


Figure 6. CVs of NiO film electrode cycled between 0 and 3.5 V at a scan rate of 5 mV/min with 1 M LiPF₆ in 1:1 EC:DMC electrolyte.

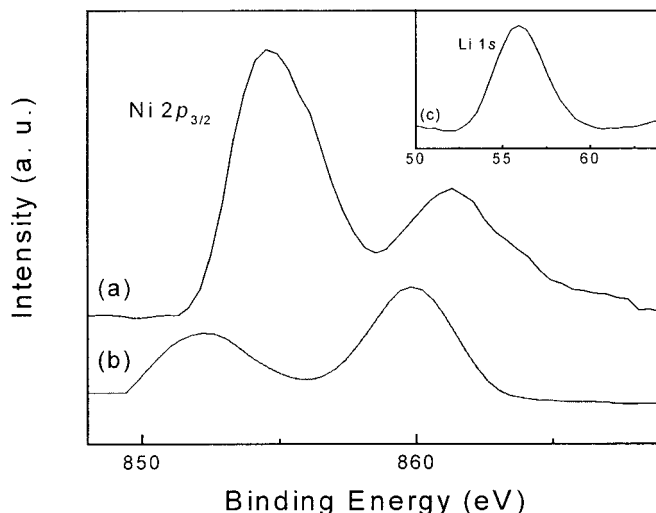


Figure 7. XPS for Ni 2p and Li 1s: (a) as-deposited NiO film electrode, (b) lithiated NiO film electrode obtained from discharge to 0.01 V, and (c) Li 1s of lithiated NiO film electrode.

In order to further understand the electrochemical mechanism of the reaction of the nanostructured NiO film with lithium, a preliminary XPS measurement was performed to examine the valence change of nickel for the NiO film before and after being lithiated. As shown in Fig. 7a, the XPS spectrum of the as-deposited film exhibits a peak at binding energy of 854.5 eV, corresponding to the Ni 2p doublet, and this binding energy is essentially the same as that found for the cubic NiO in the previous report (853.8-854.7 eV).³³ Figure 7b shows the XPS spectrum of the lithiated NiO film, which was assembled as a cell and removed from the cell after being discharged to 0.01 V. After this film was lithiated, it was found that the binding energy of Ni 2p_{3/2} shifts to about 852.4 eV, indicating a conversion of NiO to metallic nickel. The Li 1s XPS spectrum for the lithiated film is presented in the insert of Fig. 7. The binding energy peak of 55.8 eV can be assigned to Li 1s, which should be attributed to Li₂O (55.6 eV), confirming the formation of Li₂O. Our XPS result further supported that the Ni metal and Li₂O were formed in the initial discharge process.

Discussion

Nanostructured electrode materials exhibit more attractive properties compared with conventional electrode materials, such as very small particle size, large exposed surface areas, and high surface energy. These properties can reduce the diffusion distance of Li ions in solid state, enlarge the contact area between the active particles, enhance the electrochemical reaction rate, as well as results in the agglomeration of nanosized particles. Our film characterization results indicate that the NiO thin film deposited by PLA is composed of nanocrystalline NiO particles with average size of ~30 nm. The high specific capacity of the NiO thin film electrode (~700 mAh/g) can be attributed to the high surface area of the nanocrystalline NiO particles and the short diffusion distance for Li ions in the nanocrystalline NiO electrode. However, it should be noted that the morphology of the NiO particles on the film surface changed obviously both their shape and size when the NiO film/Li cell was cycled. It could be caused by the fact that the agglomeration of nanoparticles takes place on the surface of the film electrode and the larger aggregates are formed by a solid electrolyte interface (SEI) surrounded.¹⁰

To get further insight into the electrochemical properties of the NiO thin-film electrode, the reversible electrochemical mechanism of nanocrystalline NiO film with lithium is discussed in detail. Recently a new reaction mechanism for transition metal oxides with lithium was proposed by Tarascon's group⁸ and Dahn's group.¹¹

This mechanism totally differs from the classical reversible insertion/deinsertion of lithium or lithium alloying processes. Both of them have investigated CoO-based electrodes as a typical example using effective physical and electrochemical techniques. However, there are some different viewpoints between these two groups on the ability to drive the electrochemical reaction of reduced metal with lithium oxide. Tarascon's group suggested that the reduction mechanism of the metal oxide (MO) with Li involved the formation of 1-5 nm metal nanoparticles, which lead to the decomposition of Li₂O, and the metal converts back to metal oxide upon the subsequent charge. Dahn's group proposed a similar reaction mechanism for the first discharge process, including the immediate decomposition of metal oxide and the formation of nanosized metal particles. But for the subsequent charge process, they proposed that the reduced metal is oxidized to metal ions by a replacement reaction where the metal ions displace the Li ion in Li₂O via an ion-exchange process. In this reaction, Li₂O is not decomposed and the original oxygen lattice of lithium oxide is preserved. According to our experimental results and the mechanisms proposed by these two groups, we suggest that the electrochemical reaction mechanism for the nanocrystalline NiO film-based lithium cell involves the following processes.

For the first discharge process, the reaction of lithium toward NiO film takes place, in which the nanocrystalline NiO decomposes to form Ni metal and Li₂O. The resulting products were identified by our XRD and XPS measurements. The particle size of reduced Ni metal observed in our experiment could be larger than a few nanometers, which was suggested by Tarascon's group for the CoO/Li cell.⁸ They directly proved the formation of 1-5 nm metal particles by transmission electron microscopy (TEM) and considered that such small metal nanoparticles could not be observed by XRD measurement. In contrast, the diffraction peak of Ni metal was observed in our XRD pattern of the lithiated film as shown in Fig. 1c. It is difficult to assume that only the reduced metal particles in a few nanometers range can drive the electrochemical decomposition of Li₂O. In addition, there is no evidence of the diffraction peak of Li₂O in our XRD measurement, implying that the lithium oxide might be amorphous. Overall, the electrochemical reaction during the discharge process can be written as



From this reaction, the theoretical predicted capacity corresponds to 2 equiv mol of lithium ion per unit mole of NiO, but the irreversible capacity of NiO film electrode, as mentioned previously, is much larger than the predicted value. This large excess capacity could be caused by the decomposition reactions of electrolyte and formation of the SEI. Recently, Tarascon's group^{9,10} pointed out that the growth of an organic layer resulted from the reaction of the solvent electrolyte molecules and the surface of nanosized metal. This phenomenon was supported by their *in situ* TEM and selected area electron diffraction (SAED) results obtained at the end of the first discharge plateau. Our SEM image of the lithiated NiO film also revealed that the larger size and needle-like shape nanoparticles uniformly distributed on the film surface. This result provided indirect evidence for the nanoparticles agglomeration and the formation of an SEI-like layer upon cycling, although these processes need to be further clarified by TEM, infrared, and Raman spectroscopy studies being conducted in our laboratory.

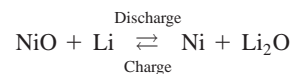
For the charging process, the XRD, XPS, and electrochemical measurements of nanocrystalline NiO film electrodes demonstrated that the reduced Ni metal displaces the lithium in Li₂O to form NiO and lithium. This electrochemical displacement reaction can be presented as follows



However, it is quite difficult for this reaction to occur under normal conditions, and the redox reaction mechanism still remains disturb-

ing, as we have discussed. For the nanocrystalline NiO film-based lithium cell, we suggest that the metallic Ni produced from the starting NiO nanoparticles on the film may still preserve the same nanosized range or reduce to smaller nanoparticles. Then the highly reactive nickel nanoparticles could convert back to NiO, accompanying the decomposition of Li₂O during the charging process.

Further cycling of the NiO film-based lithium cell proceeds via the following reversible electrochemical replacement reaction



This reaction mechanism shows that NiO could reversibly react with 2 Li per formula unit, corresponding to a reversible specific capacity of 714 mAh/g, which is very close to the observed capacity of 700 mAh/g. Since the electrochemical mechanism of the NiO film/Li cell is very complicated, more work needs to be done for the further understanding of this reaction mechanism.

Conclusion

Thin films composed of cubic NiO nanocrystalline particles having average size of about 30 nm were successfully prepared by reactive PLA in an oxygen ambient using a metallic nickel target. The NiO film electrode exhibited excellent electrochemical performance with a reversible capacity as high as 700 mAh/g at high current density and good reversibility upon cycling 100 cycles. During NiO film/Li cell discharge, the formation of the metallic nickel and Li₂O was identified by the XRD and XPS measurements. Based on our experimental results, we extend the new electrochemical mechanism proposed recently^{8,11} to the NiO film-based Li-cell. This mechanism involves the electrochemical displacement reaction of NiO with lithium, in which the nanocrystalline NiO is reduced to form metallic nickel, accompanying the formation of Li₂O. Our results also showed that metal oxide nanocrystalline films not only offer a significant advantage of improved performance of lithium-ion batteries, but also provide an ideal geometry and "clean" electrode material for fundamental research. Moreover, the successful fabrication of nanocrystalline NiO film demonstrates that PLA is a promising method for preparing thin-film electrodes of all-solid-state rechargeable lithium-ion batteries.

Acknowledgment

The authors thank Dr. W. L. Dai for his help with the XPS measurements.

References

1. J. Schoonman, *Solid State Ionics*, **135**, 5 (2000).
2. R. Vacassy, H. Hofmann, N. Papageorgiou, and M. Grätzel, *J. Power Sources*, **81-82**, 621 (1999).
3. H. Li, X. J. Huang, L. Chen, G. G. Zhou, Z. Zhang, D. Yu, Y. J. Mo, and N. Pei, *Solid State Ionics*, **135**, 181 (2000).
4. I. Kim, P. N. Kumta, and G. E. Blomgren, *Electrochem. Solid-State Lett.*, **3**, 493 (2000).
5. M. Nishizawa, K. Mukai, S. Kuwabata, C. R. Martin, and H. Yoneyama, *J. Electrochem. Soc.*, **144**, 1923 (1997).
6. N. Li, C. J. Patrissi, G. Che, and C. R. Martin, *J. Electrochem. Soc.*, **147**, 2044 (2000).
7. N. Li, C. R. Martin, and B. Scrosati, *Electrochem. Solid-State Lett.*, **3**, 316 (2000).
8. P. Poizot, S. Laruelle, S. Grugeon, L. Dupont, and J-M. Tarascon, *Nature (London)*, **407**, 496 (2000).
9. S. Grugeon, S. Laruelle, R. Herrera-Urbina, L. Dupont, P. Poizot, and J-M. Tarascon, *J. Electrochem. Soc.*, **148**, A285 (2001).
10. P. Poizot, S. Laruelle, S. Grugeon, L. Dupont, and J-M. Tarascon, *J. Power Sources*, **97-98**, 235 (2001).
11. M. N. Obrovac, R. A. Dunlap, R. J. Sanderson, and J. R. Dahn, *J. Electrochem. Soc.*, **148**, A576 (2001).
12. E. Fujii, A. Tomozawa, H. Torii, and R. Takayama, *Jpn. J. Appl. Phys., Part 2*, **35**, L328 (1996).
13. S. Passerini and B. Scrosati, *J. Electrochem. Soc.*, **141**, 889 (1994).
14. H. Sato, T. Minami, S. Takata, and T. Yamada, *Thin Solid Films*, **236**, 27 (1993).
15. H. Kumagai, M. Matsumoto, K. Toyoda, and M. Obara, *J. Mater. Sci. Lett.*, **15**, 1081 (1996).
16. P. Tomczyk, J. Wyrwa, and M. Mosialek, *J. Electroanal. Chem.*, **463**, 78 (1999).
17. M. Kitao, K. Izawa, K. Urabe, and T. Komatsu, *Jpn. J. Appl. Phys., Part 1*, **33**, 6656 (1994).

18. M. Tachiki, T. Hosomi, and T. Kobayashi, *Jpn. J. Appl. Phys., Part 1*, **39**, 1817 (2000).
19. C. Morant, L. Soriano, J. F. Trigo, and J. M. Sanz, *Thin Solid Films*, **317**, 59 (1998).
20. E. Fujii, A. Tomozawa, S. Fujii, H. Torii, M. Hattori, and R. Takayama, *Jpn. J. Appl. Phys., Part 2*, **32**, L1448 (1993).
21. T. Nishina, K. Takizawa, and I. Uchida, *J. Electroanal. Chem.*, **263**, 87 (1989).
22. K. A. Striebel, C. Z. Deng, S. J. Wen, and E. J. Cairns, *J. Electrochem. Soc.*, **143**, 1821 (1996).
23. M. Antaya, J. R. Dahn, J. S. Prestan, E. Rossen, and J. N. Reimers, *J. Electrochem. Soc.*, **140**, 575 (1993).
24. J. Zhang, J. M. McGraw, J. Tumer, and D. Ginley, *J. Electrochem. Soc.*, **144**, 1630 (1997).
25. Z. W. Fu and Q. Z. Qin, *J. Electrochem. Soc.*, **147**, 4610 (2000).
26. Z. W. Fu, J. L. Kong, and Q. Z. Qin, *J. Electrochem. Soc.*, **146**, 3914 (1999).
27. Z. W. Fu and Q. Z. Qin, *J. Phys. Chem. B*, **104**, 5505 (2000).
28. F. Ding, Z. W. Fu, M. F. Zhou, and Q. Z. Qin, *J. Electrochem. Soc.*, **146**, 3554 (1999).
29. R. Serna, C. N. Afonso, J. M. Ballesteros, A. Naudon, D. Babonneau, and A. K. Petford-Long, *Appl. Surf. Sci.*, **138-139**, 1 (1999).
30. C. N. Afonso, R. Serna, J. M. Ballesteros, A. K. Petford-Long, and R. C. Doole, *Appl. Surf. Sci.*, **127-129**, 339 (1998).
31. M. Yoshimura, K-S. Han, and S. Tsurimoto, *Solid State Ionics*, **106**, 39 (1998).
32. J. R. Dahn, T. Zheng, Y. Liu, and J. S. Xue, *Science*, **270**, 590 (1995).
33. M. Schulze, R. Reissner, M. Lorenz, M. Lorenz, U. Radke, and W. Schnurnberger, *Electrochim. Acta*, **44**, 3969 (1999).